Comparison of Battery Models Integrating Energy Efficiency and Aging for the Design of Microgrids

Corentin Boennec, Lucas Albuquerque, Bruno Sareni, Fabien Lacressonnière, Sandra Ulrich Ngueveu

Comparison of battery models integrating energy efficiency and aging for the design of microgrids

Corentin Boennec[1*], Lucas Albuquerque[1], Bruno Sareni[1], Fabien Lacressonnière[1], Sandra Ulrich Ngueveu[1,2]

[1*]LAPLACE, UMR CNRS-INPT-UPS, Universite de Toulouse, Toulouse, France.
[2]LAAS-CNRS, CNRS, INP, Universite de Toulouse, Toulouse, France.

*Corresponding author(s). E-mail(s): boennec@laplace.univ-tlse.fr;

Abstract

The robust design of microgrids based on optimization methods is a challenging process which usually requires multiple system simulations and implies the use of suitable models ensuring a good compromise between complexity and accuracy. These models also have to include the main couplings within systems, which have a major impact on design criteria and constraints. In this paper, we particularly illustrate this context with regard to the choice of battery models integrating energy efficiency and aging for the design of microgrids. Using a simple case study, we demonstrate the importance of taking into account battery capacity loss due to aging to accurately assess the microgrid's self-sufficiency and cost over its lifetime.

Keywords: Integrated optimal design, battery storage, aging, microgrids, robust design

1 Introduction

The integration of renewable energy sources in our energy production systems has become a global objective as it allows to contain global warming by limiting CO2 emissions, especially when they replace fossil fuels. All the trajectories proposed by international agencies show the importance of integrating renewable energy sources in the energy mix to reduce temperature increase in the coming decades [1, 2]. In the context of smart microgrids, Distributed Energy Systems (DES) allow the integration of renewable energy sources with both generation and consumption on site. However, the variability and unpredictability of these sources require the association of Energy Storage Systems (ESS) in order to add flexibility and reliability to the system. Among the possible ESS, battery storage systems (BSS) and in particular Li-ion batteries (LIB) are often chosen for daily storage, as they offer a good combination of energy density, maintenance level and cost per Wh of storage [3]. The design of these microgrids has oftentimes been addressed via optimization problems that aim to minimize the sum of two costs, the investment cost and the operating cost (CAPEX and OPEX) while ensuring a certain level of self-sufficiency [4–6].

Moreover, many uncertainties have to be included in this kind of design problem. Those uncertainties can be divided into two categories: aleatory uncertainties which arise from variability or stochasticity (e.g weather or energy load) and the epistemic uncertainties which originate from the lack of knowledge (e.g the intrinsic inability of models to describe reality) [7].

Regarding the epistemic uncertainties, the problem is two-fold. On one hand, a large number of numerical quantities is required for the parameterization of modeled systems (e.g., the prices of various elements within the system), and these values are sometimes uncertain in the present due to the lack of economic regulation rules but even more so in the future. On the other hand, the models used to describe the system are often simplified to facilitate optimization over long periods of time, typically spanning the system's lifetime. These simplifications lead to errors and uncertainties, which have an influence on the sizing decisions. Many of the modeling choices made in the literature, specifically battery modeling choices, are not justified or simply lack arguments to support the decision.

This paper aims to investigate the influence of the accuracy level of LIB models on simulations and constrained optimization of a microgrid. In this context, oversizing microgrid component sizes mean additional unnecessary costs for the operator of the system, while undersizing could result in reduced self-sufficiency and the need to seek alternative resources, which if unavailable, could lead to a black-out. The objective is to make modeling choices with a maximum of information regarding their impact and determine if a simple model can be identified. Therefore, in this paper, the influence of the accuracy level of LIB models is studied in order to identify the best compromise between complexity and accuracy. Several model configurations extracted from the literature [8–13] with different levels of detail will be explored and analyzed, integrating in a coupled or decoupled way energy efficiency and aging.

The remaining of the paper is organized as follows. Section 2 is devoted to the description of battery models integrating aging and energy efficiency. Section 3 presents a simple case study consisting in the robust optimization of a small microgrid with battery storage and aiming at characterizing the influence of the battery model in the design process. Section 4 gives the results associated with this case study and conclusions are presented in section 5.

2 Models description

LIB models presented and discussed in this paper are known as system models. They aim to capture some important macroscopic indicators such as state of charge (SoC), energy efficiency and state of health (SoH), while remaining suitable for optimization problems with a large number of variables. There exist more complex models to assess the aging that describe intrinsic phenomena occurring inside a LIB. Examples of these models include multi-dimensional models, single particle models, and equivalent circuit models[14].

Similarly, when it comes to energy efficiency models, more accurate models are available in the literature, such as the equivalent circuit models (e.g. Tremblay-Dessaint [15]), which are relevant for real-time control or health monitoring. However, using such models would require a finer time step. Accuracy often comes with complexity, making the aforementioned models not compliant with the sizing optimization process.

2.1 The temporal model

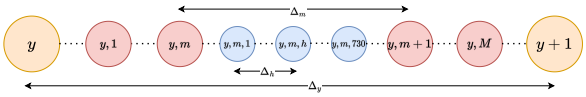

Fig. 1 Multi-scale time model and link between scales.

Our time model includes three time scales addressing different scopes. A fine scale modeled by an hourly step to capture the intra-day dynamics of the system, as well as a monthly time scale to update our cycle based aging models and finally a long scale with an annual step for investment management. The link that is made between these time scales can be seen in Figure 1.

The set of hours, months and years are then respectively defined as $h \in \mathbb{H} = \{1..H\}$, $m \in \mathbb{M} = \{1..M\}$, $y \in \mathbb{Y} = \{1..Y\}$, with associated time-steps Δ_h, Δ_m and Δ_y verifying $\Delta_y = 12\Delta_m = 8760\Delta_h$.

2.2 The energy model

The energy model defines the State of Charge (SoC $\in [0, 1]$) of the battery during its interaction with the system. Specifically, here the LIB

are operated within the limit of $SoC^{min} = 0.2$ and $SoC^{max} = 0.8$.

$$SoC_{h+1} = SoC_h - \frac{(\eta^{ch} \cdot P_h^{ch} + \eta^{dch^{-1}} \cdot P_h^{dch}) \cdot \Delta_h}{E(t)} \tag{1}$$

Equation (1) from [16] governs the battery SoC at hourly intervals Δ_h, where $P_h^{ch} \leq 0$ and $P_h^{dch} \geq 0$ respectively denotes the LIB charge/discharge power at hour h. These variables do not coexist, meaning if one is non-zero the other one is. This equation has few parameters: the charging or discharging power for the hour h P_h^{ch}, P_h^{dch}, the energy efficiency η and the capacity $E(t)$ of the battery in [kWh] at instant t.

In order to take into account the influence of the energy efficiency on the design of the LIB, two models have been implemented.

2.2.1 Constant efficiency

The first model is simply a constant efficiency "model" with $\eta^{ch} = \eta^{dch}$. The chosen value of 99% lies within the efficiency range of the model from [13] to ensure that the simpler model efficiency is of the same order of magnitude, thereby avoiding any effects resulting from a significantly different average efficiency.

2.2.2 Polynomial efficiency

This second model, originating from [13], differentiates between charge and discharge efficiency and describes the degradation of efficiency as a polynomial function of the C_{rate}:

$$\eta^{ch}(C_{rate}) = 0.0033 \cdot C_{rate}^2 - 0.0297 \cdot C_{rate} + 0.99814 \tag{2}$$

$$\eta^{dch}(C_{rate}) = 0.002232 \cdot C_{rate}^2 - 0.0246 \cdot C_{rate} + 1 \tag{3}$$

Even if these two equations have different coefficients, they have the same form and are second-degree equations. They both depend on the C_{rate}, which is the applied current in terms of the battery capacity. So a 1C current would discharge a battery in an hour and a 2C current would discharge it in 30 minutes. By considering both the charge and discharge efficiencies, this model can better predict the performance of LIB under various operating conditions. One could note that when operating the battery with an hourly time step and a state of charge (SoC) within the range of [0.2, 0.8], the C_{rate} remains within the interval of [0, 0.6]. This implies that $\eta^{ch} \in [0.982, 0.998]$ and $\eta^{dch} \in [0.986, 1]$.

2.3 The aging models

The aging models represent the State of Health evolution of the battery (SoH $\in [0, 1]$) during its interactions with the system. The SoH represents the actual capacity of the battery related to its capacity at the beginning of life. In this study the replacement threshold corresponding to the battery End Of Life (EOL) is set to 80%, which means the battery is replaced when SoH falls below 80%. It is known that stationary storage can be pushed to around 40% [17]. However, the models used in this study do not take account of the rapid degradation phase occuring at the EOL. The degradation rate can substantially increase shortly after our 80% threshold, with the curve forming a "knee" [18] depending on the battery usage during its first life. This phenomenon can be explained by hidden electrochemical mechanisms that are not significant in terms of capacity degradation during the beginning of a battery life but can become the main degradation factor with aging. The "knee" is therefore a combination of multiple complex mechanisms such as the Loss of Lithium Inventory (LLI) and Loss of Active Materials (LAM) at the electrodes. Therefore, we limit this study to an area in which aging is better known. Nevertheless, with the development of Second Life battery aging models [19, 20], the impact of the EOL threshold should be further studied as well as the control strategies when the battery falls down beyond the "knee" inflection point.

In this study, four aging models have been implemented. They are presented in an increasing order of captured aging dynamics.

2.3.1 Fixed lifetime model (FL)

The Fixed Lifetime (FL) model takes into account only calendar aging. For this model, the SoH is simply a function of the elapsing time, assuming that the battery has a fixed lifetime.

$$\Delta_{cal}(t) = 1 - e^{t \cdot c_{cal}} \tag{4}$$

with $c_{cal} = 1.49 \cdot 10^{-6}$ and t being the time in hours.

The calendar degradation model is expressed as a linear degradation extracted from the time stress function of [9] and similar to [21]. Indeed, the parameter c_{cal} is obtained by isolating the time-related stress factor for one hour. This is achieved analytically by fixing the various model parameters to the reference conditions, thereby isolating the degradation caused by one hour of calendar aging. The SoH is then computed as:

$$SoH_{h+1} = SoH_h - \Delta_{cal}(\Delta_h) \tag{5}$$

The next models implement at least a cycle aging factor related to battery usage in addition to calendar aging. While the cycling degradation model is different for each aging model, this calendar degradation model is shared with the next two models.

2.3.2 Energy Throughput model (ET)

The Energy Throughput (ET) model [8] allows to estimate the SoH according to a function of a total amount of exchangeable energy and the part of it already exchanged with the system. The maximum exchangeable energy E_{tot}^{ex} depends on N_{tot}^{cycle} the achievable number of cycles for a fixed Depth of Discharge (DoD) and on the nominal energy E^{nom} of the battery at 100% SoH,

$$E_{tot}^{ex} = 2 \cdot N_{tot}^{cycle}(DoD^{max}) \cdot DoD^{max} \cdot E^{nom} \tag{6}$$

where DoD^{max} is the maximum depth that a half cycle (charge or discharge) can reach. It is calculated via:

$$DoD^{max} = SoC^{max} - SoC^{min} \tag{7}$$

In order to determine the parameter N_{tot}^{cycle}, the Number of Cycles-to-Failure (NCF) curve from [9] was used, giving the number of cycles before reaching $EOL = 80\%$. For implementation purposes, the relation $N_{EOL}^{cycle} = N_{tot}^{cycle} \times (1 - EOL)$ needs to be define so that once the quantity E_{tot}^{ex} is exchanged, the battery ends up at $SoH = 80\%$. The hourly cycle degradation is then computed according to the following equation, with P_h being the LIB charge/discharge power in one hour h.

$$\Delta_{cyc}(h) = \frac{(|P_h^{ch}| + P_h^{dch}) \cdot \Delta_h}{E_{tot}^{ex}} \tag{8}$$

The SoH is finally computed as:

$$SoH_{h+1} = SoH_h - \Delta_{cyc}(h) - \Delta_{cal}(\Delta_h) \tag{9}$$

Note that the model accuracy strongly depends on the depth of the representative cycle, here DoD^{max}. If DoD^{max} differs from the DoD imposed by the battery profile, then the accuracy of the aging model will be lower.

2.3.3 Rainflow model (RF)

In this model inspired from [10] the per cycle degradation is evaluated by a Rainflow count. The method consists in calculating a fatigue as a function of a SoC profile $\overrightarrow{SoC}$, in order to update the SoH. More precisely, the total fatigue is obtained by adding the fatigue associated to each half-cycle (charge or discharge) of the profile. The induced fatigue is a function of the depth of the half-cycle in question. In order to obtain this profile, the calculation of this fatigue is periodically performed once a month (every Δ_m). The $\overrightarrow{SoC_{y,m}}$ profile of the previous month SoC must be processed to extract a vector containing the DoD of each half-cycle performed during that month. The extraction process is detailed in Fig. 2.

The value of the fatigue generated (10) during the past month is then obtained via (10) where $\overrightarrow{DoD}$ is the vector of DoDs associated with the SoC profile:

$$\Delta_{cyc}(m) = \sum_{i=1}^{|\overrightarrow{DoD}|} \frac{1}{2 \cdot NCF(\overrightarrow{DoD}_i)} \tag{10}$$

The factor 2 in the denominator comes from our choice to consider half-cycles. The NCF function provides, via the NCF curve supplied by the manufacturer, the number of cycles achievable for a given DoD before EOL. Finally, adding the calendar degradation gives the equation for a monthly update:

$$SoH_{m+1,1} = SoH_{m,H} - \Delta_{cyc}(m) - \Delta_{cal}(\Delta_m) \tag{11}$$

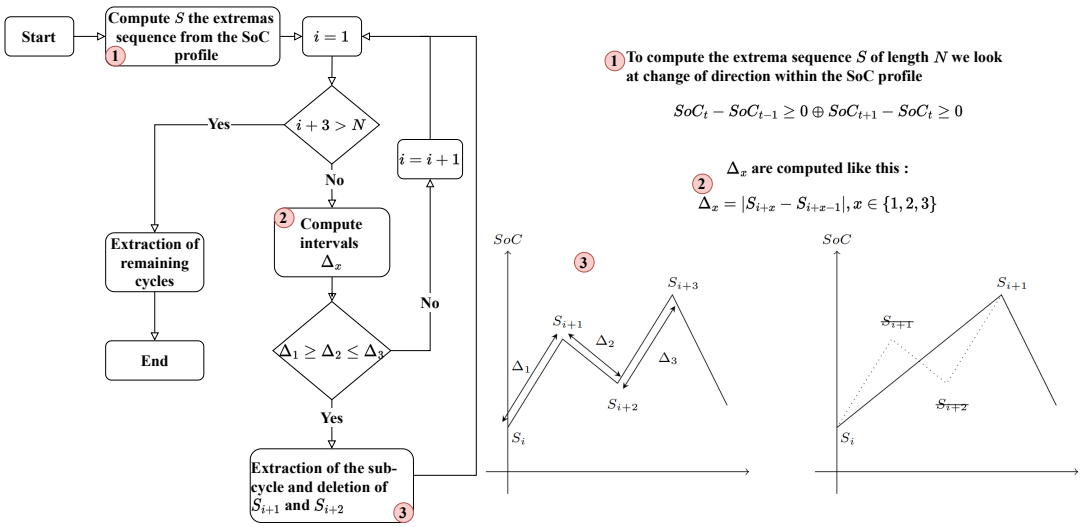

Fig. 2 Rainflow cycle extraction flowchart.

2.3.4 Semi-Empirical model (SE)

This model from [9] incorporates empirical and physical degradation parameters. It differs from the other models because it takes account of several electrochemical reactions taking place within the battery at the beginning of its life, caused by the consumption of lithium-ions and electrolyte to form the passivation layer called Solid Electrolyte Interphase (SEI). This layer is essential for the battery longevity, as it protects the graphite from direct contact with the electrolyte, but continues to grow and thus degrades the battery capacity during its life [22]. The general formula to compute the degradation for a new battery is given by :

$$SoH_t = \alpha_{sei} \cdot e^{-\beta_{sei} \cdot fd_t} + (1 - \alpha_{sei}) e^{-fd_t} \quad (12)$$

with $\alpha_{sei} = 5.75 \cdot 10^{-2}$ and $\beta_{sei} = 121$ being empirical coefficients (fitted for an NMC battery in [12]) describing SEI formation and fd_t being the global stress undergone by the battery until time t depending on four parameters: the average depth of discharge $\overline{DoD}$, the elapsed time t, the average state of charge $\overline{SoC}$ and the temperature T. Hence, we consider fd^{unit} as the unit equivalent associated with a single half-cycle. Therefore, fd_t is defined as the sum of fd^{unit} for each half-cycle up to the instant t. The fd^{unit} parameter is calculated via the following equation:

$$fd^{unit} = [\frac{1}{2} S_{DoD}(DoD) + S_t(t)] S_{SoC}(\overline{SoC}) S_T(T) \quad (13)$$

where S_x are the stress functions defined in [9] which allow the calculation of the stress associated with each degradation factor. Their parameters are empirically estimated for an NMC battery in [12].

In this paper, we consider that the LIB is placed in a regulated thermal environment as close as possible to $T_{ref} = 298.15K$. Hence, despite the influence of the temperature on the battery aging [23]), this parameter is excluded from our study (in Eq. (12), the value of $S_T(T)$ is constant and equal to 1).

Finally, Eq. (12) is computed each month with an updated value for fd_t. The update is done monthly by adding to fd_t all the fd^{unit} associated with the cycles that have been performed during the past month and is computed as follows:

$$fd_{t+\Delta_m} = fd_t + \sum_{i=1}^{N_{cycle}(m)} fd_i^{unit} \quad (14)$$

with $N_{cycle}(m)$ being the amount of half-cycles extracted from the SoC profile using the process detailed in Fig. 2 and associated to the month m.

A brief summary of the models features can be found in Table 1. It should be noted in this table that the first two aging models can easily be implemented in Mixed Integer Linear Programming (MILP)-based optimization methods [5, 21], while the last two using the Rainflow counting algorithm are highly non-linear and do not have a closed form [24], making them unusable in these methods commonly used for microgrid design.

Table 1 Aging models considered features.

Model	FL	ET	RF	SE
Calendar	√	√	√	√
Cycling	-	√	√	√
Cycle Amplitude	-	-	√	√
Average SoC	-	-	-	√
SEI Formation	-	-	-	√
Linearization	√	√	-	-

2.3.5 Calibration of the models for meaningful comparison

In order to make our models as comparable as possible, we have chosen to configure them using the same data from [9]. The calendar part of the degradation model is extracted by isolating the calendar stress from the *Semi-Empirical* model. The cycling part is calibrated using the *NCF* curve for an NMC battery provided in the same reference. For the *Energy Throughput* model, we take from this *NCF* curve the number of cycles achievable for a DoD of 60% (DoD^{max}), thus obtaining the parameter N_{EOL}^{cycle}. Finally the *Rainflow* model directly uses the *NCF* curve.
It is worth noting that although all models have a calendar aging term, only the one in the *Semi-Empirical* model is influenced by the average SoC level.

2.4 Coupling between energy and aging models

The term "coupling" in this paper refers to the influence of battery aging on its electrical characteristics (i.e. capacity, internal resistance). Most works in the literature consider the aging and energy efficiency models in parallel, without any link and without any modification of the battery internal parameters during aging (e.g [5, 25–31]). This is done for simplicity reasons and because it increases the complexity of the optimization problem formulation which becomes nonlinear. Nevertheless, an approach to overcome these difficulties is proposed in [32].

In our study, four types of coupling are considering as follows:

- The absence of coupling between energy and aging models.
- The energy (E) coupling, which induces a loss of capacity for the LIB defined as follows: $E(t) = E^{nom} \cdot SoH_t$.
- The internal resistance (R) coupling, which induces a loss of efficiency by a linear decrease as proposed in [11] or [21] via: $\eta(SoH_t) = \eta^{ini} - (0.2303 \cdot (1 - SoH_t))$ with an initial efficiency η^{ini} given by the energy models from section 2.2.
- The E and R (ER) coupling which applies both simultaneously.

Finally when the R coupling is considered, the polynomial efficiency is computed as follows:

$$\eta^{ch} = \eta^{ch}(C_{rate}) - (0.2303 \cdot (1 - SoH_t)) \quad (15)$$

$$\eta^{dch} = \eta^{dch}(C_{rate}) - (0.2303 \cdot (1 - SoH_t)) \quad (16)$$

It should be noted that $\eta^{ch}(C_{rate}, SoH_t) \in [0.935, 0.998]$ and $\eta^{dch}(C_{rate}, SoH_t) \in [0.94, 1]$ for the polynomial model.

3 Description of our case study

3.1 The microgrid

A small microgrid with storage represented in Fig. 3 is considered to observe the impacts of the battery modeling with regard to the various techno-economic indicators of the system. The choice of a simple case study operated with a trivial management policy allows us to conduct our analyses over a 20-year horizon with an hourly time step. The system sizing variables are:

- The battery size: E_{bat} [kWh].
- The peak power of the photovoltaic array: P_{pv} [kWp].

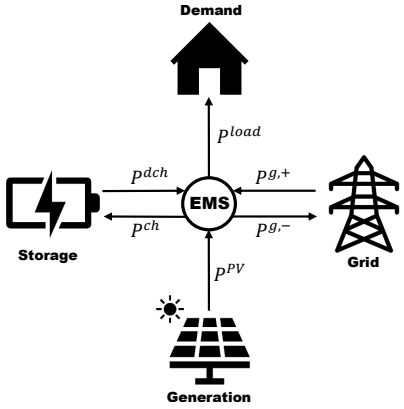

Fig. 3 Power flow diagram of our simple microgrid

- The subscribed power which, if exceeded, will generate additional costs: P_{sub} [kVA].

3.2 Techno-economical metrics

The system was evaluated with two main indicators: the system cost and its self-sufficiency level.

3.2.1 Self-sufficiency

The Renewable Energy Share (RES) is a metric of the system self-sufficiency. It measures the share of energy supplied by the PV panels in the total energy consumption of the system. Since the system has two possible suppliers, PV panels or grid, this share is obtained from its complement (the grid share):

$$RES = 1 - \frac{\sum P^{g,+}}{\sum P^{load}} \tag{17}$$

With $P^{g,+}$ being the power provided by the grid each hour and P^{load} the load demand.

3.2.2 System costs

The cost metric used in this study is the Net Present Value (NPV). For its calculation C_y^i, C_y^o are defined respectively as the investment and operating costs for year y. C_Y^s is the residual value of the equipment, calculated at the end of the time horizon $y = Y$ (non-zero only for $y = Y$). For the battery, a linear decrease of its value is considered, reaching 0% at EOL. Finally, the discount rate τ is set at 4.5%. The cost C_y^{base} was deliberately excluded from the calculations (the cost of meeting demand over the simulation horizon by relying exclusively on the grid) because it is independent on the battery modeling choices. The NPV is then defined by (18).

$$NPV = \sum_{y=1}^{Y} \frac{(-C_y^i - C_y^o + C_y^s)}{(1+\tau)^y} \tag{18}$$

3.3 Details about the simulation environment

To simulate the microgrid and conduct the analysis on the models, certain requirements must be fulfilled. This includes obtaining input data to evaluate the production and demand at each time step, as well as determining the values of the sizing and operating variables. This section outlines the approach taken in this study to address these considerations.

Scenarios

Regarding the scenarios, a set $\mathcal{S}$ of 16 scenarios of 20-year with an hourly time step was used. They provide for each hour the energy demand and solar radiation. In the context of this study, the use of scenarios is three-fold. Firstly we want to account for aleatory uncertainties, secondly we need to use credible, reality-like data and finally we try to avoid limiting the results to a specific case, thus making them more general. Their generation is done according to a Markov process described in [33] with data from *Ausgrid* of 20 consumers over the years 2010 to 2012 [34]. This method has the advantage of allowing the generation of a large number of artificial data from a reduced number of initial data while keeping the consistency and the correlation between the different time series. More details can be found in the appendix A.

Sizing

Concerning the sizing, assuming that the magnitude of the observed effects should vary with the size of the system components, a set of values is considered for the sizing parameters. The subscribed power P_{sub} is set to 10 kVA. The values of the couple (P_{pv}, E_{bat}) are generated by a Sobol sequence [35] whose bounds are min = (0,100), max = (0,160) in order to cover the space under

consideration as uniformly as possible while keeping the flexibility to increase the sizing amount without having to rerun all the previous simulations. Thus 1024 designs are generated and the point (0,0) is added afterwards thus constituting the design set $\mathcal{D}$. By associating these sizing to the scenarios, a set of 16400 configurations (1025 sizing x 16 scenarios) is provided as input to simulate the microgrid.

Operation policy

Finally the decisions regarding the power flows are taken by a simple rule based controller. The rules are as follows:

- In case of surplus ($P_h^{load} - P_h^{pv} < 0$) the battery is charged. The excess is sold to the grid if SoC reaches SoC^{max}.
- In case of a deficit ($P_h^{load} - P_h^{pv} > 0$) the battery is discharged. The grid takes over if SoC reaches SoC^{min}.

Altogether and combined, those elements allow us to simulate the microgrid on a large and diverse set of sizing configurations (16400).

3.4 Toward robust constrained optimization

We remind that the problem is to find the cheapest (NPV) robust design (battery and solar panels) within the search space able to ensure a certain level of self-sufficiency. The aleatory uncertainties are here addressed via a set of scenarios $\mathcal{S}$ and in our case the search space is represented by the set $\mathcal{D}$.

The robust optimization problem is defined as follows:

$$\begin{aligned} \min_{d\in\mathcal{D}} \quad & \sum_{s\in\mathcal{S}} \frac{NPV(d,s)}{Card(\mathcal{S})} \\ \text{s.t.} \quad & \sum_{s\in\mathcal{S}} \frac{\delta_\varphi(RES(d,s))}{Card(\mathcal{S})} \geq \beta \\ & \delta_\varphi(x) = \begin{cases} 1 & \text{if } x \geq \varphi \\ 0 & \text{otherwise} \end{cases} \end{aligned} \tag{19}$$

This formulation consists in finding the design within $\mathcal{D}$ that allows to obtain the minimum cost on average over all the $\mathcal{S}$ scenarios, while ensuring a level φ of self-sufficiency for at least a fraction β of the scenarios. This is a Conditional Value at Risk (CVaR) formulation [36], which incorporates uncertainties while providing flexibility in self-sufficiency and robustness. It can also be noted that this formulation is linearizable [37]. For the following results the β value is set to 15/16 to ensure the robustness.

As the $\mathcal{D}$ set only consists of 1025 points, we have chosen to address the optimization exhaustively. This approach was adopted for a fair comparison between the models, as these different models would involve different optimization techniques, including exact and heuristic optimization methods, which would blur the conclusions. Our aim in defining this type of optimization problem formulation is to provide an analysis of the modeling factors that allow a model to efficiently determine feasible solutions and identify the best one among them. Ultimately, we want to determine the model with the lowest complexity that successfully combines these two attributes.

3.5 Key data associated with costs

Table 2 provides some important cost data used for our simulations and analysis.

4 Results

Before addressing the case of robust constrained optimization we here present some preliminary analysis.

4.1 Comparison of aging models on artificial SoC profiles

In this section, aging models are compared according to the artificial SoC profiles of Fig. 4. Those profiles, which are voluntary simple, allow characterizing the effect of the following variables related to the cycles: average state of charge, depth of discharge and frequency.

Fig. 5 shows the strong effect of the average SoC only modeled in the *Semi-Empirical* model in which, above the reference value (here set to 0.5) accelerates aging, while on the contrary, is slowed down when the battery is operated below the reference value (see profile 2 compared with profile 3 and profile 4 compared with profile 5).

Note that if, out of all the profiles, the *Semi-Empirical* model is generally the one with the

Table 2 Main cost parameters.

	Cost	extra informations	Reference
Subscription cost	203 €/year for 10 kVA	Data from the reference has been made continuous by inter/extrapolation for analysis purposes	[38]
Electricity tariffs	0.23 €/kWh	VAT included for peak hours (with a 0.75 factor for off-peak hours).	[38]
Cost of exceeding the subscription limit	10.2 €/h	Most offers trip the installation rather than charging for the excess usage; here we model the second option.	[39]
PV panels	1300 €/kWp		[40]
Li-ion cells	300 €/kWh		[40]
Selling price	0 €/kWh		

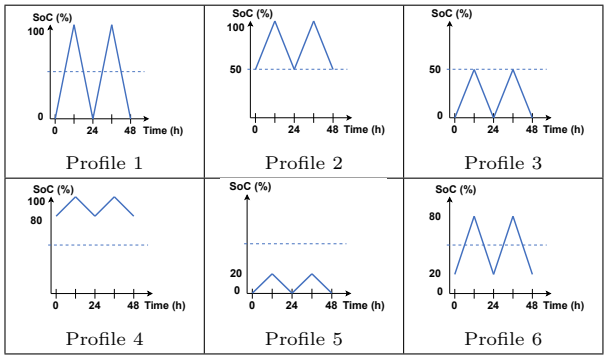

Fig. 4 Artificial SoC profiles over 48 hours - Profiles 7-12 have the same amplitude as 1-6 but twice the frequency.

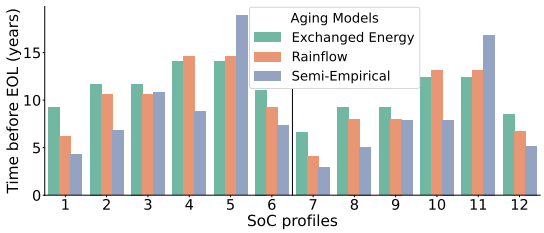

Fig. 5 Lifetime before reaching EOL of batteries undergoing artificial SoC profiles from Fig. 4.

shortest lifetime because it incorporates an additional irreversible degradation due to the formation of the SEI. The only cases contradicting this statement are those where this effect is compensated by the effect of the average SoC mentioned in the previous paragraph. This is observable on profiles 3 and 5 as well as their equivalent 9 and 11.

4.2 Reference model

In order to evaluate the relevance and accuracy of the different models presented in this paper, a reference is needed to compare the results. Considering the observation period required for such a system, associated with the high level of investment, it seems difficult to have real data available as a reference. If we take into account the need to observe a large number of sizing operations carried out under comparable conditions, it then becomes impossible to access real data as a reference.

Therefore, among the possible model combinations presented in the previous sections, the finest model was chosen as the reference, which consists of the *Semi-Empirical* model combined with the *polynomial efficiency* model, with (ER) coupling linking capacity and efficiency to the aging. This choice is motivated by the fact that all the degradation dynamics for NMC batteries identified by [41] are captured and validated in [9] by excellent experimental results.

4.3 Measuring the deviation from the reference model

Here, we measure the gaps in the assessment of the techno-economic indicators of our models compared with the reference. We quantify the percentage deviation from the reference, according to different metrics. For each model configuration (aging, coupling and energy model), 16400 simulations are performed.

Fig. 6 displays part of our results (we only show results for ER coupling and no coupling and the result shown only include the energy model

Constant Efficiency). It can be seen that the metric primarily impacted by the level of accuracy of the aging model seems to be the NPV. Meanwhile the RES is mainly affected by the choice of incorporating or not the coupling.

Secondly, we observe that the dispersion of the deviations for the cost metric is quite large and that its amplitude increases when the models incorporate fewer features, up to approximately $[-30, +30]\%$ with the *Fixed Lifetime* model. The deviation can be positive or negative although it is mostly negative. Not incorporating the coupling increases the trend towards the negative part. These underestimations of the cost are mostly due to an overestimation of the life expectancy of the battery, which ultimately leads to fewer replacements (or a higher salvage value). It could be noted that the efficiency model is of low importance by examining the right-hand side of Fig. 6b. This implies that the results obtained with the *Polynomial Efficiency* are very similar. Consequently, we will not display them. Indeed, the distribution of error induced by implementing a *Constant Efficiency* model is highly limited.

Finally, we can measure the effect of modeling the coupling alone by comparing the reference to its equivalent without coupling. We note that the magnitude of the effect on NPV is smaller than the one due to aging models. On the other hand, we can see that the magnitude of the effect on RES is totally due to this factor.

4.4 Quantitative differences but qualitative similarities?

The quantitative deviations of the battery models investigated in the paper have been characterized in the previous section with regard to the RES and NPV criteria. We now examine the qualitative differences of those models with respect to the microgrid configurations and scenarios of Section 3.3. For each model, 16400 simulations are carried out and sorted in ascending order of the considered criterion (i.e. RES or NPV). The similarity of the rankings between two models i and j is estimated using the Spearman correlation defined as follows:

$$r_{ij} = 1 - \frac{6}{n(n^2-1)} \sum_{k=1}^{n} d_k^2 \qquad (20)$$

where $n = 16400$ is the total number of tests and d_k denotes the difference between two rankings in the sorts. A value of r_{ij} close to 1 indicates similar rankings (i.e. same behavior between models i and j) while a value of r_{ij} close to 0 means that both models are totally uncorrelated.

Table 3 compares 16 battery model configurations to the reference with respect to the r_{ij} coefficient and NPV criterion. It can be seen that Spearman coefficients are relatively high leading to similar behaviors.

Without surprise, the lowest coefficient is between the *Fixed Lifetime* model (considered as the less quantitatively accurate) and the *Semi-Empirical* model (supposed to be the most quantitatively accurate). Both *Rainflow* and *Energy Throughput* models perform similarly with a short advantage for the latter. It is noticeable that it is easier for the models to rank input configurations rather than sizing (with an average cost over the scenarios), this is observable in Table 3 through higher scores on the first result line than on the second one. This can be explained by the fact that some scenarios have higher demands and are unanimously more expensive than others. It is therefore easy to rank them, thus increasing the correlation score.

The Spearman coefficient results associated with the RES are rounded to one while not being strictly perfect. But the minor inversions happening still result in a very high correlation which implies an almost perfect similarity between all models. This can be justified by the small quantitative differences and low dispersion noted for that criterion in Fig. 6.

4.5 Conclusions of the preliminary analysis

Previous sections contains results that tend to show that despite having different behaviors and aging trajectories, resulting in distant quantitative evaluations in terms of NPV (cf. Fig. 6), the models propose similar rankings but not identical. It was also shown that the main aspect in order to assess the self-sufficiency of the system rather than the aging model is the capacity reduction induced by the aging here named (E) coupling. One could argue that since the capacity reduction is a direct function of the SoH governed by the aging model, the aging model should be of great importance. In

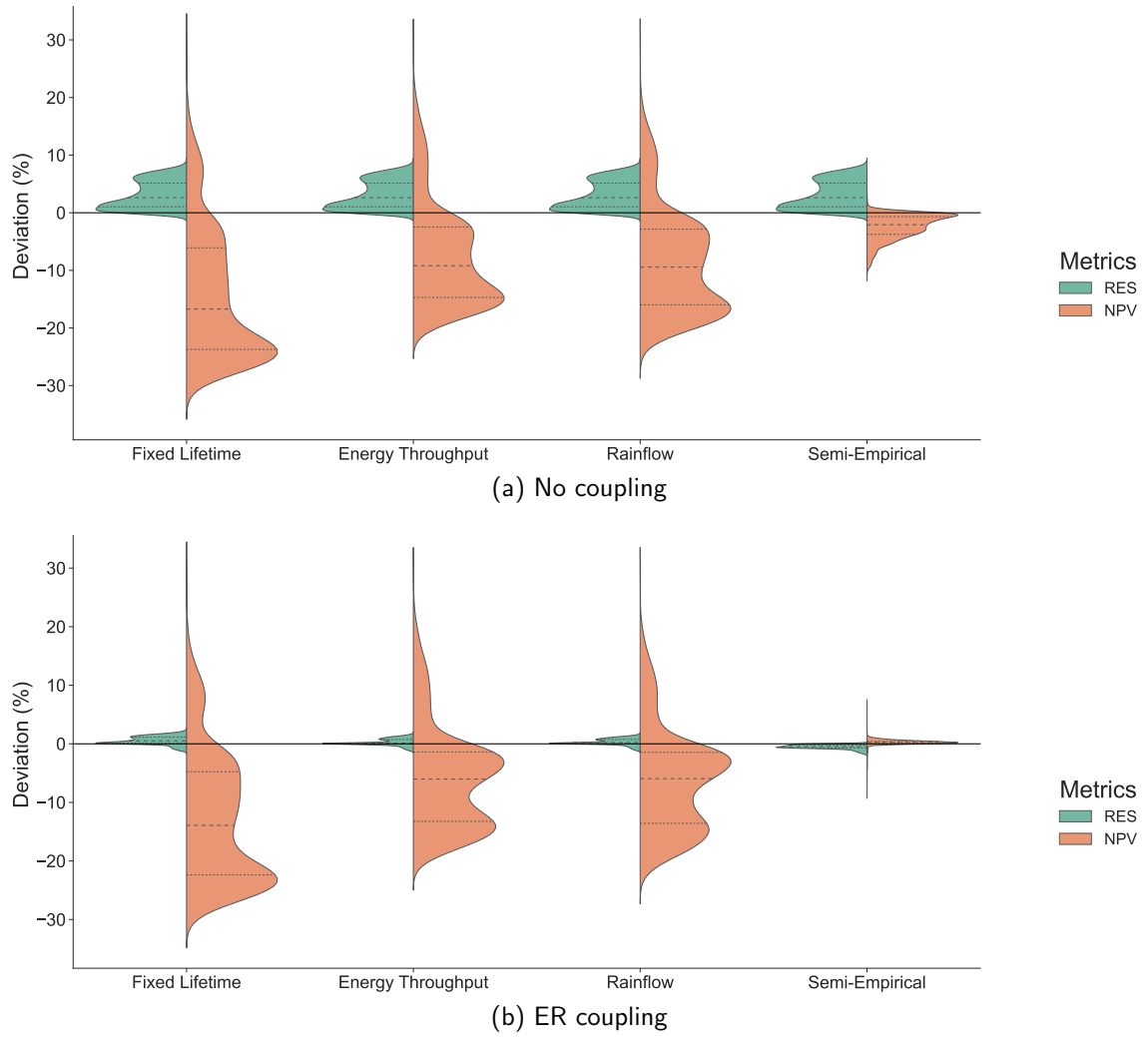

Fig. 6 Distribution of the deviation in percentage from the reference for different models and computed as: $\frac{(val-ref)\cdot 100}{ref}$. The horizontal dotted lines represent the quartiles. The efficiency model considered here is the *Constant* one.

order to answer this question, the distribution of the average SoH over the 16400 input configurations is provided in Fig. 7. During the simulations the SoH level and thus the available battery capacity remains on average relatively similar between the models. On the other hand, the replacement of the batteries occurs at different frequencies. This will result in significant differences on the system costs, but much less on their self-sufficiency.

Considering these preliminary results, it is important to understand whether a simple model can lead to similar results as the finest one for the design problem with a self-sufficiency constraint. For this purpose, we will now address the case of optimization using the formulation introduced in Section 3.4.

4.6 Constraint satisfaction front line comparison

Considering our problem formulation, we first want to identify if the models agree on the set of solutions that fulfills the constraints. Assuming that the NPV and RES criteria are in most cases antagonistic, the cheapest feasible solution is expected to be found on the edge of the constraint satisfaction front line. Therefore, an error regarding the estimation of this line by a model could

Table 3 Spearman correlation coefficient for each model configuration with regard to the reference. The *NPV* and *RES* columns use the ranking of input configurations (16400 combinations of sizing and scenarios), while the *NPV mean* and *RES mean* columns use the ranking of sizing (for each sizing, the average across different scenarios is used) Legend: ∅ is the absence of coupling and ER means both couplings (E and R)

Aging	Efficiency	Coupling	NPV	Averaged NPV	RES	Averaged RES
Fixed Lifetime	Constant	∅	.87	.82	1	1
		ER	.88	.83	1	1
	Polynomial	∅	.87	.82	1	1
		ER	.88	.83	1	1
Energy Throughput	Constant	∅	.93	.91	1	1
		ER	.94	.92	1	1
	Polynomial	∅	.93	.91	1	1
		ER	.94	.92	1	1
Rainflow	Constant	∅	.93	.90	1	1
		ER	.93	.92	1	1
	Polynomial	∅	.92	.90	1	1
		ER	.93	.92	1	1
Semi-Empirical	Constant	∅	1	1	1	1
		ER	1	1	1	1
	Polynomial	∅	1	1	1	1
		ER	1	1	1	1

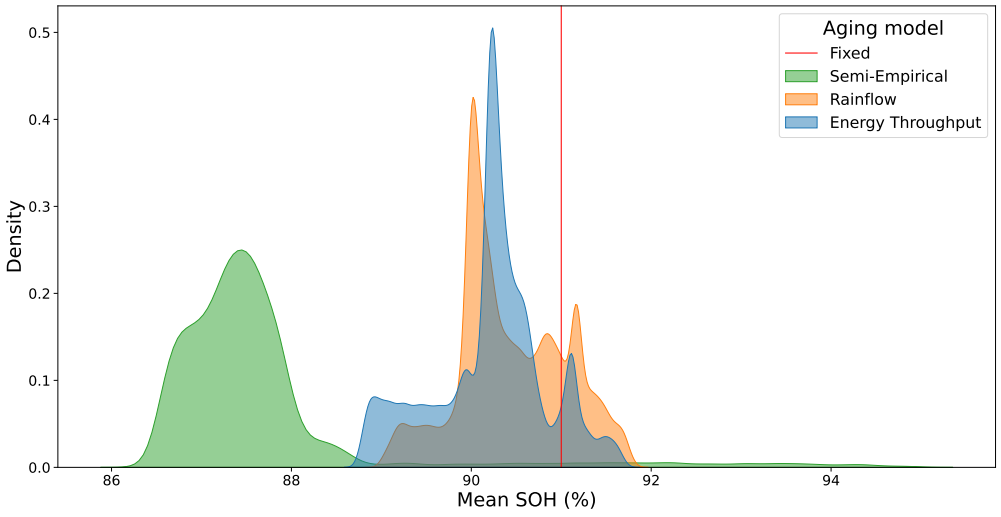

Fig. 7 Mean SoH Distribution. Red line stand for the Fixed Lifetime model.

result in a very different and distant optimal solution proposal within the search space. To observe this line, every design within $\mathcal{D}$ over the scenarios of $\mathcal{S}$ was simulated. Then, the front satisfaction line for a given RES constraint as defined in (19) is drawn. We chose to display the comparison for an arbitrary set of five levels of self-sufficiency φ in order to draw conclusions for different case studies.

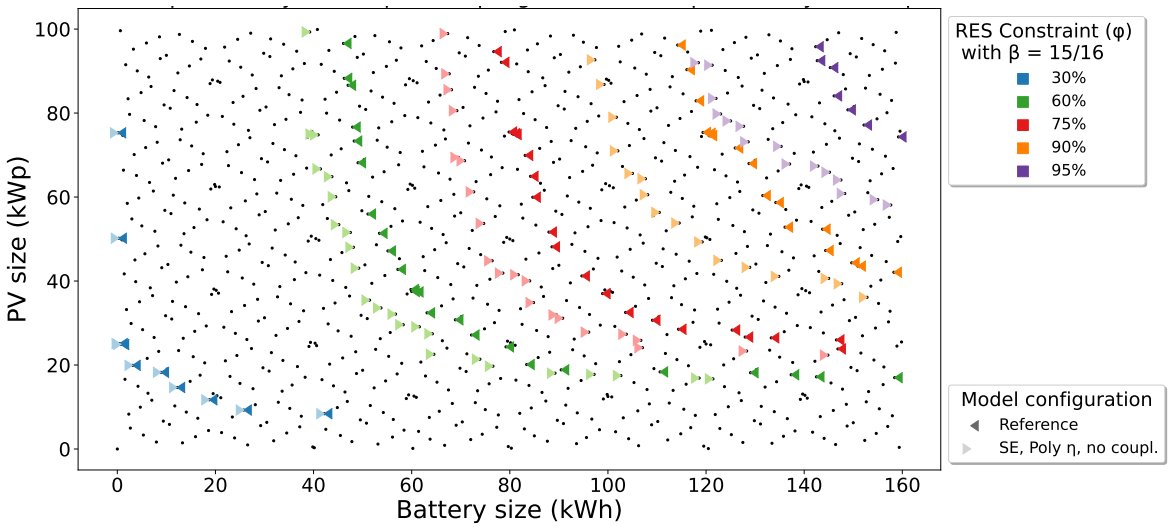

Fig. 8 Constraint satisfaction front line comparison, the effect of the coupling between energy efficiency and aging. Every black dot is a design from $\mathcal{D}$. Leftward-pointing triangles stand for the reference and rightward-pointing triangles stand for the reference model but without coupling.

Influence of energy-aging coupling

As expected, Fig. 8 shows that the absence of coupling (and especially (E) coupling) results in a huge overestimation of the RES, leading to the consideration of many solutions that would not meet the constraint. It is noticeable that this effect increases with the constraint level φ, while no difference is observed for $\varphi = 30\%$, a difference of more than 20 kWh in battery sizing for a constraint level $\varphi = 90\%$ is perceived. This effect was expected considering the results from Section 4.3. The absence of (E) coupling leads to an overestimation of the average battery capacity during its life, making the task of ensuring self-sufficiency easier since more energy capacity is available.

Influence of the energy model

On the other hand, Fig. 9 shows a small effect in the opposite direction with the *Constant* energy efficiency model providing a slightly worse efficiency on average than the *Polynomial* energy efficiency model. This results in an underestimation of the RES, leading not to consider some feasible solutions. However, the intensity of this effect is much lower than that observed for (E) coupling.

Influence of the aging model

Finally, it can be observed from Fig. 10 and Fig. 11 that the LIB aging model seems to be of relatively minor importance when it comes to estimating the constraint satisfaction front line. This conclusion had already been observed in previous quantitative analyses. Ultimately, this translates into very good results achieved with the simplest model configurations (roughly modeling aging and efficiency) as long as (E) coupling is integrated.

In conclusion, we can see that the decisive factor for correctly estimating the self-sufficiency constraint is the (E) coupling. In fact, a simple aging and/or efficiency model can be associated with it and still provide a very good estimate of the self-sufficiency constraint. However, it is likely that lowering the battery replacement threshold $SoH_{threshold}$ would result in bigger averaged SoH gaps between models. This would imply bigger gaps in capacity which would, in the end, lead to an inaccurate evaluation of the self-sufficiency. Consequently it is important to remind that this study is conducted on first life batteries operated in the [100-80]% SoH range, it could be interesting to investigate similar analyses on wider SoH ranges and on second-life batteries.

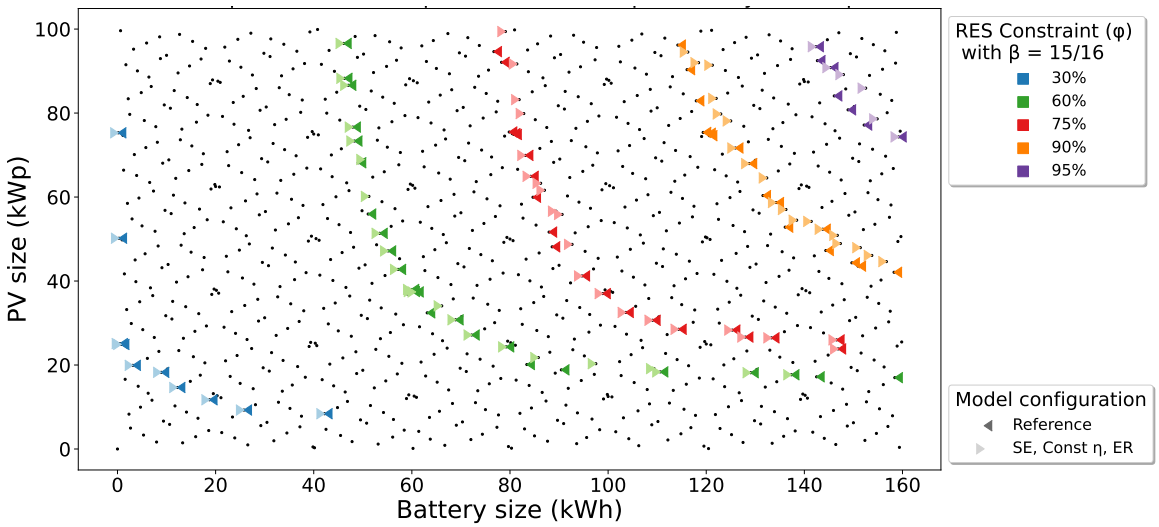

Fig. 9 Constraint satisfaction front line comparison, the effect of energy efficiency model. Every black dot is a design from $\mathcal{D}$. Leftward-pointing triangles stand for the reference and rightward-pointing triangles stand for the reference model with the *Constant* energy efficiency model.

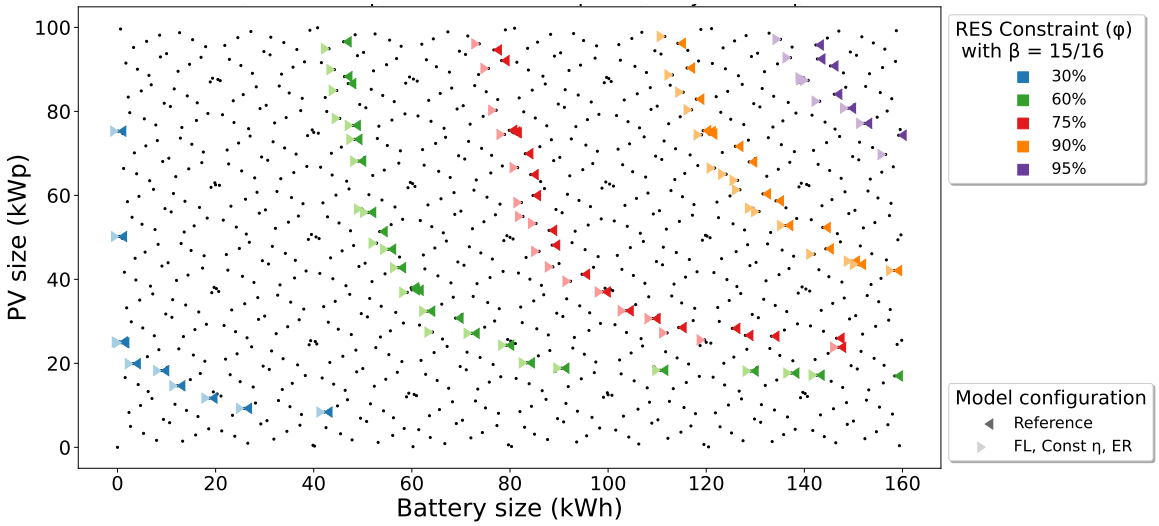

Fig. 10 Constraint satisfaction front line comparison, the simplest aging model (FL) and efficiency model (Constant Efficiency) with coupling ER compared to the reference

4.7 Search space map

Having shown that the integration of (E) coupling is necessary, we will now only consider models incorporating it. Fig. 12 shows a NPV map over each possible sizing for each aging model and each energy efficiency model with (ER) coupling.

As seen on the maps, the cost mainly varies with the PV axis for all models. However, when comparing the optimal zone for each model, *Fixed Lifetime* tends to find lower costs for solutions with relatively high PV peak powers and battery sizes, since it overestimates the battery lifetime by only considering calendar aging.

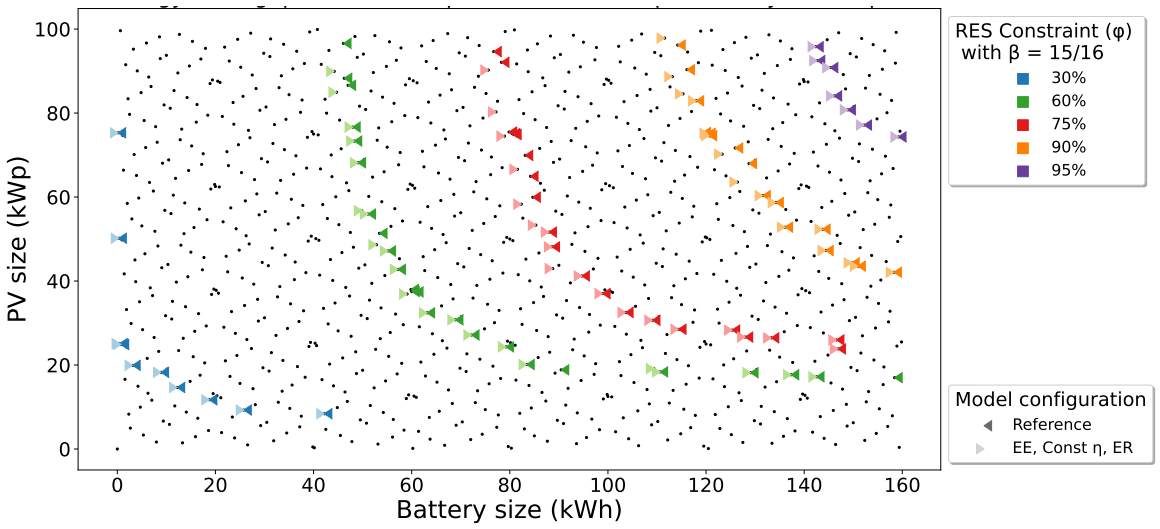

Fig. 11 Constraint satisfaction front line comparison, a simple model with coupling ER compared to the reference

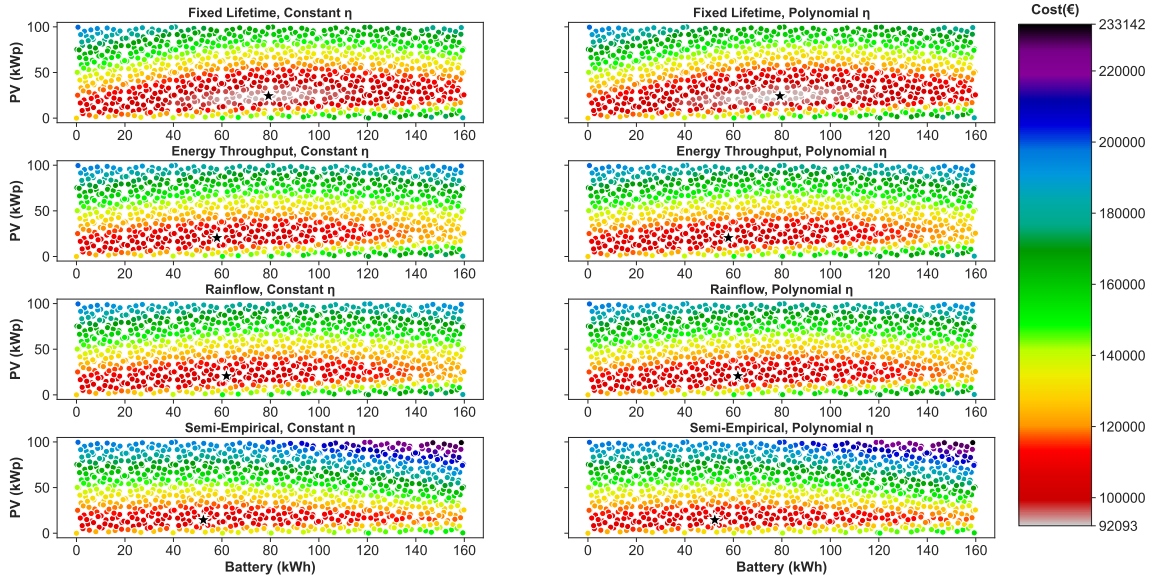

Fig. 12 NPV values over the search space for each energy and aging models with ER coupling. The black star represent the optimal solution within each search space.

As for *Rainflow* and *Energy Throughput*, they show similar results since both model calculations are dependent on the SoC variations during battery usage, meaning that the SoH is a direct image of the SoC profile. Fig. 7 confirms this last statement, since the SoH distribution for both models shows similar patterns. The results obtained with the reference model indicate that the other three models underestimate the actual NPV in some regions, mainly towards solutions with bigger solar panels and batteries. This is due to the fact that for the *Semi-Empirical* model, over-sized solar panels tend to maintain high levels of SoC within the batteries, penalizing the calendar and cycling aging factors which are dependent

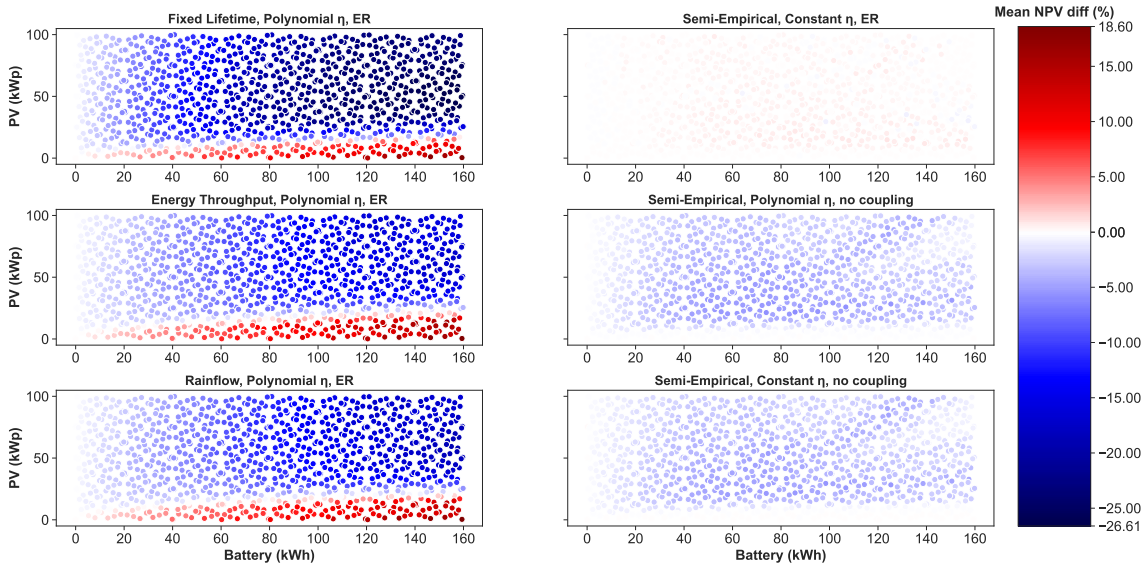

Fig. 13 NPV gap map (in percentage) between a sample of model configurations and the reference. The gap is computed for a given model x as $100 \cdot (NPV_x - NPV_{ref})/NPV_{ref}$

on the average SoC level. On the other hand, the other aging models overestimate the cost compared to the reference for small-sized solar panels, and the more the battery represents a significant portion of the system cost, the more pronounced this effect becomes. In this case, the SoC will generally remain low, which will result in slower aging for the reference model. These conclusions are highlighted in the left column of Fig. 13.

Fig. 12 also gives important insights for the study of optimal solutions found for different RES constraints. If a given model is capable of finding the constraint satisfaction front line correctly, since the NPV map patterns are the same, even if their quantitative results are not, then the model will be able to find the optimal solution. As seen before, this means that even if they are off on the quantitative aspect, they manage to correctly rank the models.

Fig. 12 provides an overview of the NPV solutions landscape. It has been observed that these landscapes have similar patterns but with different NPVs for a given sizing. We propose to investigate the extent and causes of these differences through Fig. 13.

Firstly, it is evident that the effects are strengthened by increasing the battery size, while they are diminished or even eliminated if the battery size is small or zero. Secondly, on the left column, it can be observed that there is a tipping line, beyond which the effects change qualitatively. This tipping is explained by a SoC level that is sufficiently high so that the stress factor S_{SOC} of the *Semi-Empirical* model has an accelerating effect on aging. For a given battery size, there exists a solar panel size around which the battery is either frequently full or frequently empty. Beyond a zone close to this band, the effect does not appear to be influenced by the size of the solar panel. It seems that there is a narrow equilibrium point around which the stress factor S_{SoC} of the *Semi-Empirical* model is at reference and so is ineffective.

Finally, it can be observed that the effects in the right column are quantitatively much weaker than those observed in the left column. This reveals that the main factor for evaluating the NPV of the solutions is the aging model rather than the coupling or the energy efficiency model. This is obviously true when comparing the aging model with itself but with different coupling configurations. The statement is valid as long as the battery model precisely predicts the average SoH during its usage and the time before EOL.

4.7.1 Sensitivity to PV panels & battery costs

As it turns out, meeting self-sufficiency constraints does not depend on system costs, so the conclusion regarding the sufficiency of coupling to estimate constraint front-lines remains valid. In this case, it is reasonable to assume that only the pattern of the objective landscape will be affected by variations in system costs. This pattern will presumably be influenced by the relative prices of different system components. Therefore, to ensure methodological consistency, the decision was made to keep the electricity price fixed and vary the battery price at three levels (+50%, +0%, -50%) and the solar panel price at two levels (+0%, -50%) providing a combination of 6 system costs set.

Fig. 14 shows a comparison of landscape patterns for two models: the reference model on the right and the *Energy Throughput*, *Constant Efficiency*, and (ER) coupling on the left, for six sets of prices. The color bar is adjusted to each plot to better highlight the landscape pattern rather than the quantitative value. Through observation, it is noted that the landscapes display a consistent degree of similarity across all instances. However, the error amplification and the extent of variation in landscapes become more pronounced as the battery price increases in relation to the prices of electricity and solar panels, as evident from rows 3 and 6. In some specific cases, with high constraint levels and high battery costs, this can lead to greater errors in the optimal solution proposed by the simple model.

4.7.2 Sensitivity to feed-in tariffs

It is also important to study if these results hold in a case where it is possible to sell energy to the grid, since most energy markets worldwide have already implemented the necessary regulations to permit this action. To explore this issue, a simple model was used where the price of the feed-in tariffs is set as a percentage of the energy retail price [42]. In this case study, an arbitrarily value of 50% of the buying price was chosen. Aside from the quantitative aspect, this value is expected to be of little importance since it will not change the way the battery is operated. Fig. 15 displays the NPV values over the research space with feed-in tariffs. Obviously the possibility of selling supplementary electricity makes the investment in solar panels much more attractive. It is also interesting to note that the models display similar NPV patterns. However a potential problem can be perceived: despite producing similar patterns, the *Fixed Lifetime* model finds that buying a battery is profitable. This is not the case for the optimal solution of the other models. This discrepancy arises from an overestimation of the battery's lifetime. While this simple model illustrates this effect with the feed-in tariffs used for the simulation, it is very likely that other models could also reveal this issue under specific price conditions.

Fig. 16 shows that the effect on the NPV gap map is similar to the previous case study without the implementation of feed-in tariffs. This similarity is explained by the battery being operated in the same way, leading to the same model errors and differences in life expectancy. However, the percentage of underestimation increases since the CAPEX gap represents a greater share of the total cost in solutions with feed-in tariffs, where prices are inevitably equal to or lower than those in simulations without feed-in tariffs.

4.8 Location of the optimal solutions

Fig. 17 shows the best solution for a sample of four model configurations and the optimal solution found for the reference model considering multiple RES constraints. For display purposes we chose to link the solutions forming the constraint satisfaction front line of the reference model. The configuration associating the *Fixed Lifetime* aging model with no coupling to the *Constant Efficiency*, represented with filled squares, is the simplest one and performs quite badly for different reasons, depending on the level of constraint. In case of high self-sufficiency, this model is unable to accurately estimate the constraint front line. Thus the optimal is found within solutions with smaller PV and battery sizes. On the contrary, in case of low self sufficiency (here 30%) the error comes from the fact that the optimal solution is found with a bigger battery because its durability is overestimated. This effect was already seen in Fig. 12. When the same model configuration with ER coupling is considered, represented with empty circles, the error regarding the low self-sufficiency constraint remains, because that it is not due to

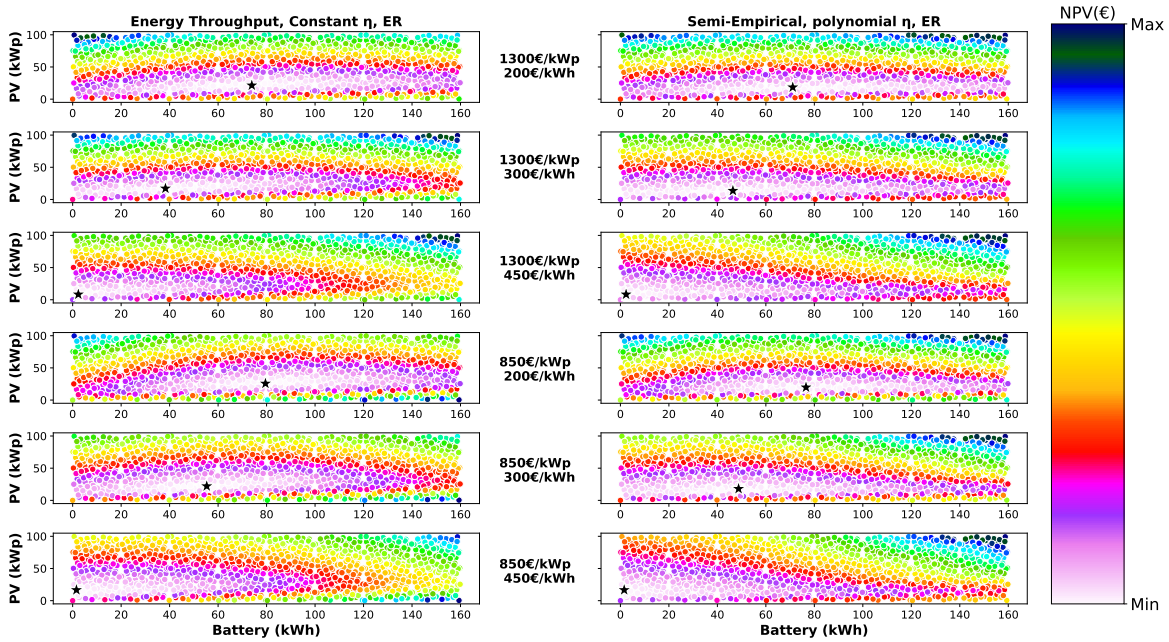

Fig. 14 Comparison of the NPV landscape between two model configurations across 6 price sets. Each map has its own color scale to better display the landscape pattern.

the coupling effect. However, when it comes to higher self-sufficiency, the model tends to estimate the optimal area decently while never finding the exact solution. The results for the model configuration *Energy Throughput*, *Constant* η with (ER) coupling and the *Rainflow*, *Polynomial* η with (ER) coupling (respectively the diamond and empty upward triangles) are quite satisfactory. Indeed, at any self-sufficiency level, the estimation of the optimal solution is fairly accurate. The former and simpler of the two models is even able to provide the optimal solution in the case of 90% RES level. It is worth noting its good performance, achieving good estimation by roughly modeling the aging and energy efficiency dynamics. The optimal solution for the reference model in the case where $\varphi = 30\%$ is surprisingly not found alongside from the constraint satisfaction line. This implies that there is some kind of equilibrium here where it is possible to make profit by improving the self-sufficiency. However this is true for the specific set of values shown in Table 2 and would be different for a different balance between those costs.

5 Conclusion

In this paper, we have provided a comprehensive understanding of the impact of LIB modeling choices in the context of microgrid design with regard to NPV and self-sufficiency optimization. Several battery models coupling energy efficiency and aging, characterized by different levels of accuracy and complexity, have been compared. The analysis of those models on a simple microgrid with battery storage for different sizing configurations and multiple scenarios of PV production and electricity consumption has allowed us to draw the following conclusions. On one hand, representing the coupling between aging and energy efficiency (especially the loss of battery capacity) is essential for determining robust microgrid solutions with respect to NPV minimization under a self-sufficiency constraint. On the other hand, when this coupling is integrated, using simple models for the energy efficiency (i.e. *Constant* average efficiency) and for aging (i.e. *Energy Throughput*) is then sufficient for identifying the feasible solutions and approximate the optimal sizing. However, for assessing the quantitative value of those solutions, a more accurate aging model (i.e. *Semi-Empirical*) is required. Finally, it should be noted that these

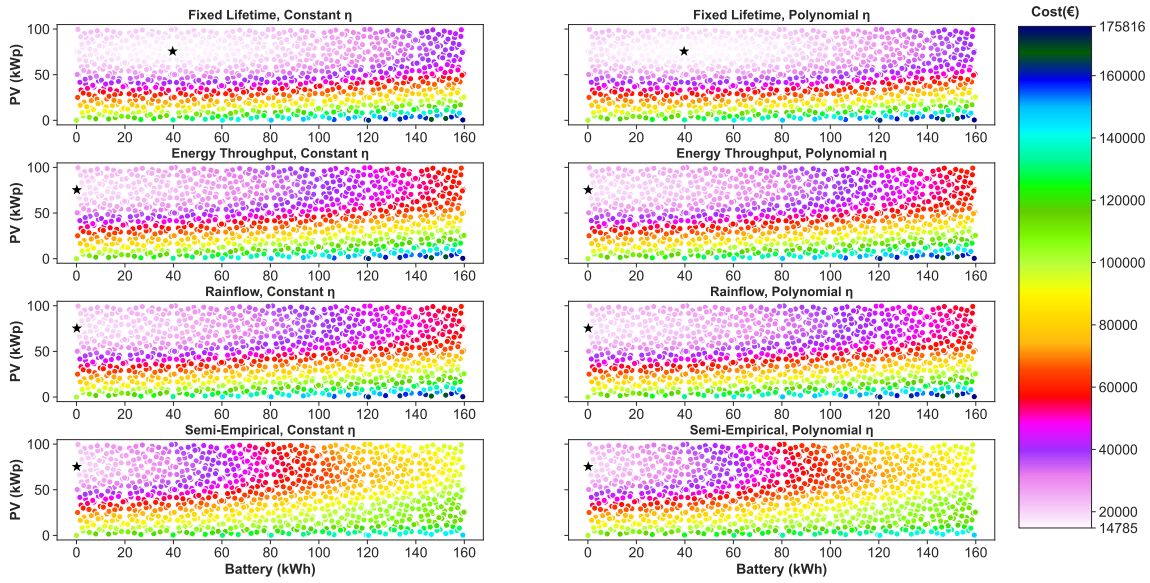

Fig. 15 NPV values over the research space with feed-in tariffs for each energy and aging models with ER coupling. The black star represent the optimal solution within each search space.

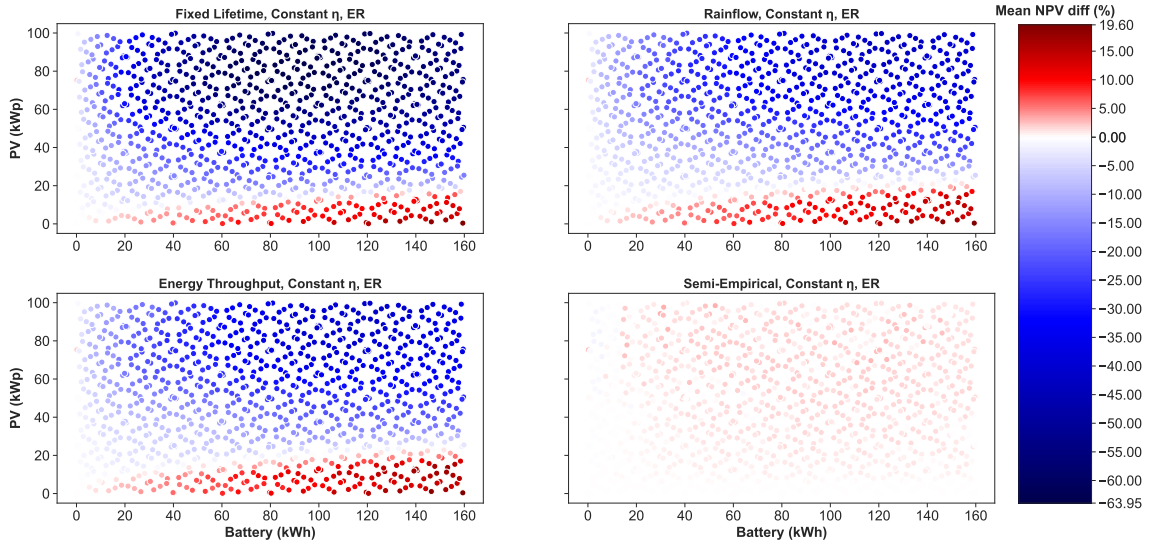

Fig. 16 NPV gap map (in percentage) with feed-in tariffs between a sample of model configurations and the reference. The gap is computed as $100 \times (NPV_x - NPV_{ref})/NPV_{ref}$

conclusions were only confirmed for the considered input data and battery technologies used in the paper. Their generalization needs to be either confirmed or refuted by future studies investigating other technologies and more complex microgrid architectures.

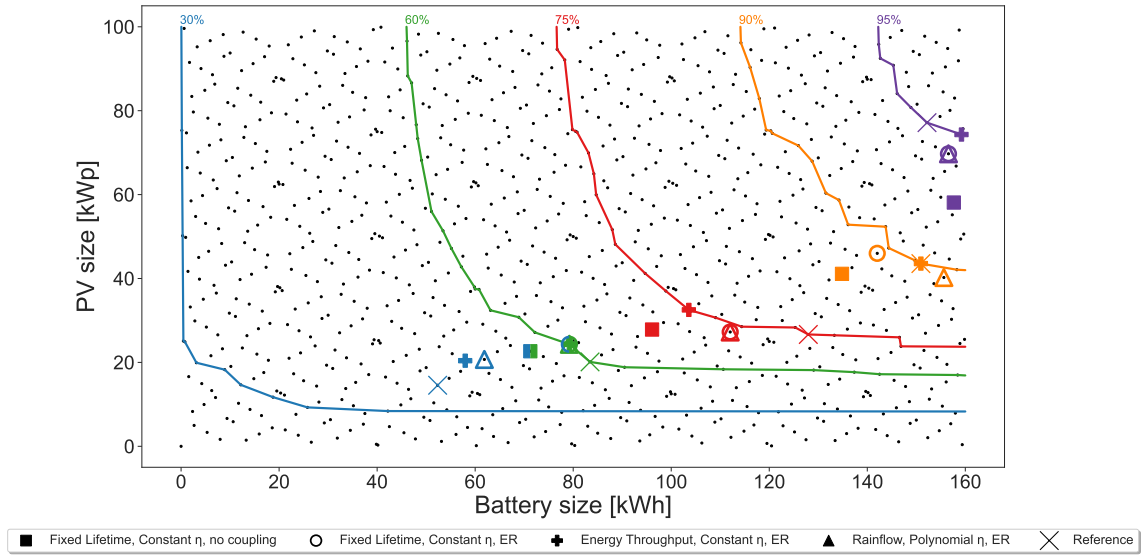

Fig. 17 Optimal solution for different models compared to the reference optimal over various constraint self-sufficiency levels. Colored lines represent the constraints satisfaction front lines for the reference model.

6 Data Availability statement

To produce the results and figures presented in this paper, we utilized data and code. All the necessary files are available in the repository [43]. The repository contains a comprehensive collection of resources, including the cleaned data associated with Ausgrid's clients from [34]. Moreover, it contains the scripts required to use this data for generating scenarios.

The repository offers access to a file containing 50 scenarios produced with the aforementioned script. Specifically, the first 16 scenarios displayed on A1 and A2 were utilized in the scripts to generate the results showcased in this paper. Additionally, the repository contains a complete version of the micro-grid simulation package employed in our studies.

In order to mimic the parameterization of our battery models, we also provide the cycle-to-failure curve. This curve is crucial for configuring most of our aging models.

Furthermore, we have included the simulation script within the repository. This script enables the replication of the grid simulations and the exploitation of the results to generate the various figures and tables found in this paper (excluding the appendix). Finally we have provided a separate set of result files which is the result of our simulations for those who want to skip the simulation phase and only analyze their outputs.

References

[1] IEA: Net Zero by 2050 - A Roadmap for the Global Energy Sector. Technical report, Paris. https://www.iea.org/reports/net-zero-by-2050 Accessed 2023-03-09

[2] IPCC: Global Warming of 1.5°C: IPCC Special Report on Impacts of Global Warming of 1.5°C Above Pre-industrial Levels in Context of Strengthening Response to Climate Change, Sustainable Development, and Efforts to Eradicate Poverty. Cambridge University Press, UK (2022). https://doi.org/10.1017/9781009157940

[3] Tarascon, J.-M., Patrice, S.: Electrochemical Energy Storage vol. 1. ISTE Editions Ltd. and Wiley, France (2015)

[4] Cuisinier, E., Bourasseau, C., Ruby, A., Lemaire, P., Penz, B.: Techno-economic planning of local energy systems through optimization models: a survey of current

methods. International Journal of Energy Research **45**(4), 4888–4931 (2021) https://doi.org/10.1002/er.6208

[5] Marocco, P., Ferrero, D., Martelli, E., Santarelli, M., Lanzini, A.: An MILP approach for the optimal design of renewable battery-hydrogen energy systems for off-grid insular communities. Energy Conversion and Management **245**, 114564 (2021) https://doi.org/10.1016/j.enconman.2021.114564

[6] Spertino, F., Ciocia, A., Di Leo, P., Fichera, S., Malgaroli, G., Ratclif, A.: Toward the complete self-sufficiency of an nzebs microgrid by photovoltaic generators and heat pumps: Methods and applications. IEEE Transactions on Industry Applications **55**(6), 7028–7040 (2019) https://doi.org/10.1109/TIA.2019.2914418

[7] Rocquigny, E., Devictor, N., Tarantola, S.: Uncertainty Settings and Natures of Uncertainty. In: Rocquigny, E., Devictor, N., Tarantola, S. (eds.) Uncertainty in Industrial Practice, pp. 199–211. John Wiley & Sons, Ltd, Chichester, UK (2008). https://doi.org/10.1002/9780470770733.ch14

[8] Bindner, H., Cronin, T., Lundsager, P.: Lifetime modelling of lead acid batteries (2005)

[9] Xu, B., Oudalov, A., Ulbig, A., Andersson, G., Kirschen, D.S.: Modeling of Lithium-Ion Battery Degradation for Cell Life Assessment. IEEE Transactions on Smart Grid **9**(2), 1131–1140 (2018) https://doi.org/10.1109/TSG.2016.2578950

[10] Shi, Y., Xu, B., Tan, Y., Kirschen, D., Zhang, B.: Optimal battery control under cycle aging mechanisms in pay for performance settings. IEEE Transactions on Automatic Control **64**(6), 2324–2339 (2019) https://doi.org/10.1109/TAC.2018.2867507

[11] Redondo-Iglesias, E., Venet, P., Pelissier, S.: Efficiency degradation model of lithium-ion batteries for electric vehicles. IEEE Transactions on Industry Applications **55**(2), 1932–1940 (2019) https://doi.org/10.1109/TIA.2018.2877166

[12] Mathews, I., Xu, B., He, W., Barreto, V., Buonassisi, T., Peters, I.M.: Technoeconomic model of second-life batteries for utility-scale solar considering calendar and cycle aging. Applied Energy **269**, 115127 (2020) https://doi.org/10.1016/j.apenergy.2020.115127

[13] Li, K., Tseng, K.J.: Energy efficiency of lithium-ion battery used as energy storage devices in micro-grid. In: IECON 2015 - 41st Annual Conference of the IEEE Industrial Electronics Society, pp. 005235–005240 (2015). https://doi.org/10.1109/IECON.2015.7392923

[14] Xu, B.: The role of modeling battery degradation in bulk power system optimizations. MRS Energy & Sustainability **9**(2), 198–211 (2022) https://doi.org/10.1557/s43581-022-00047-7

[15] Tremblay, O., Dessaint, L.-A.: Experimental Validation of a Battery Dynamic Model for EV Applications. World Electric Vehicle Journal **3**(2), 289–298 (2009) https://doi.org/10.3390/wevj3020289

[16] Carpentier, P., Chancelier, J.-P., Lara, M., Rigaut, T.: Algorithms for two-time scales stochastic optimization with applications to long term management of energy storage. working paper or preprint (2019). https://hal.science/hal-02013969

[17] Braco, E., San Martin, I., Sanchis, P., Ursúa, A., Stroe, D.-I.: Health indicator selection for state of health estimation of second-life lithium-ion batteries under extended ageing. Journal of Energy Storage **55**, 105366 (2022) https://doi.org/10.1016/j.est.2022.105366

[18] Attia, P.M., Bills, A., Planella, F.B., Dechent, P., Reis, G., Dubarry, M., Gasper, P., Gilchrist, R., Greenbank, S., Howey, D., Liu, O., Khoo, E., Preger, Y., Soni, A., Sripad, S., Stefanopoulou, A.G., Sulzer, V.: Review—"knees" in lithium-ion battery aging trajectories. Journal of The Electrochemical Society **169**(6), 060517 (2022) https://doi.org/10.1149/1945-7111/ac6d13

[19] Seger, P.V.H., Coron, E., Thivel, P.-X., Riu,

D., Cugnet, M., Genies, S.: Open data model parameterization of a second-life li-ion battery. Journal of Energy Storage **47**, 103546 (2022) https://doi.org/10.1016/j.est.2021.103546

[20] Braco, E., Martín, I.S., Sanchis, P., Ursúa, A.: Analysis and modelling of calendar ageing in second-life lithium-ion batteries from electric vehicles. In: 2022 IEEE International Conference on Environment and Electrical Engineering and 2022 IEEE Industrial and Commercial Power Systems Europe (EEEIC / I&CPS Europe), pp. 1–6 (2022). https://doi.org/10.1109/EEEIC/ICPSEurope54979.2022.9854784

[21] Vermeer, W., Mouli, G.R.C., Bauer, P.: Optimal sizing and control of a pv-ev-bes charging system including primary frequency control and component degradation. IEEE Open Journal of the Industrial Electronics Society **3**, 236–251 (2022) https://doi.org/10.1109/OJIES.2022.3161091

[22] Pinson, M.B., Bazant, M.Z.: Theory of sei formation in rechargeable batteries: Capacity fade, accelerated aging and lifetime prediction. Journal of The Electrochemical Society **160**(2), 243 (2012) https://doi.org/10.1149/2.044302jes

[23] Vermeer, W., Chandra Mouli, G.R., Bauer, P.: A comprehensive review on the characteristics and modeling of lithium-ion battery aging. IEEE Transactions on Transportation Electrification **8**(2), 2205–2232 (2022) https://doi.org/10.1109/TTE.2021.3138357

[24] Shi, Y., Xu, B., Tan, Y., Zhang, B.: A Convex Cycle-based Degradation Model for Battery Energy Storage Planning and Operation. In: 2018 Annual American Control Conference (ACC), pp. 4590–4596 (2018). https://doi.org/10.23919/ACC.2018.8431814

[25] Jiang, W., Wang, X., Huang, H., Zhang, D., Ghadimi, N.: Optimal economic scheduling of microgrids considering renewable energy sources based on energy hub model using demand response and improved water wave optimization algorithm. Journal of Energy Storage **55**, 105311 (2022) https://doi.org/10.1016/j.est.2022.105311

[26] Sigalo, M.B., Pillai, A.C., Das, S., Abusara, M.: An Energy Management System for the Control of Battery Storage in a Grid-Connected Microgrid Using Mixed Integer Linear Programming. Energies **14**(19), 6212 (2021) https://doi.org/10.3390/en14196212

[27] Wu, X., Zhao, W., Wang, X., Li, H.: An MILP-Based Planning Model of a Photovoltaic/Diesel/Battery Stand-Alone Microgrid Considering the Reliability. IEEE Transactions on Smart Grid **12**(5), 3809–3818 (2021) https://doi.org/10.1109/TSG.2021.3084935

[28] Nottrott, A., Kleissl, J., Washom, B.: Storage dispatch optimization for grid-connected combined photovoltaic-battery storage systems. In: 2012 IEEE Power and Energy Society General Meeting, pp. 1–7. IEEE, San Diego, CA (2012). https://doi.org/10.1109/PESGM.2012.6344979

[29] Murray, P., Orehounig, K., Grosspietsch, D., Carmeliet, J.: A comparison of storage systems in neighbourhood decentralized energy system applications from 2015 to 2050. Applied Energy **231**, 1285–1306 (2018) https://doi.org/10.1016/j.apenergy.2018.08.106

[30] Gabrielli, P., Gazzani, M., Martelli, E., Mazzotti, M.: Optimal design of multi-energy systems with seasonal storage. Applied Energy **219**, 408–424 (2018) https://doi.org/10.1016/j.apenergy.2017.07.142

[31] Li, B., Roche, R., Miraoui, A.: Microgrid sizing with combined evolutionary algorithm and MILP unit commitment. Applied Energy **188**, 547–562 (2017) https://doi.org/10.1016/j.apenergy.2016.12.038

[32] Seger, P.V.H., Rigo-Mariani, R., Thivel, P.-X., Riu, D.: A storage degradation model of Li-ion batteries to integrate ageing effects in the optimal management and design of an isolated microgrid. Applied Energy **333**, 120584 (2023) https://doi.org/10.1016/j.apenergy.2022.120584

[33] Radet, H., Sareni, B., Roboam, X.: Generation of energy demand and pv production profiles based on markov chains for the design and operation of microgrids. 14th International Conference of TC-Electrimacs Committee, Nancy, France, 2022 (2022)

[34] Ausgrid: Solar home electricity data. https://www.ausgrid.com.au/Industry/Our-Research/Data-to-share/Solar-home-electricity-data. Accessed: 2022-02-15

[35] Sobol, I.M.: On the distribution of points in a cube and the approximate evaluation of integrals. USSR Computational Mathematics and Mathematical Physics **7**(4), 86–112 (1967) https://doi.org/10.1016/0041-5553(67)90144-9

[36] Rockafellar, R.T., Uryasev, S.: Optimization of conditional value-at-risk. The Journal of Risk **2**(3), 21–41 (2000) https://doi.org/10.21314/JOR.2000.038

[37] Rockafellar, R.T., Uryasev, S.: Conditional value-at-risk for general loss distributions. Journal of Banking & Finance **26**(7), 1443–1471 (2002) https://doi.org/10.1016/S0378-4266(02)00271-6

[38] EDF: Grille de prix de l'offre de fourniture d'électricité *Tarif Bleu*. https://particulier.edf.fr/content/dam/2-Actifs/Documents/Offres/Grille_prix_Tarif_Bleu.pdf. Accessed: 2022-02-15

[39] l'énergie, C.: Barème des tarifs reglementés de vente d'électricité applicables aux consomateurs résidentiels en France métropolitaine continentale. https://www.cre.fr/content/download/23276/file/210114_2021-08_Proposition_Tarifaire_Annexe_B-Baremes.pdf. Accessed: 2022-02-15

[40] Petkov, I., Gabrielli, P.: Power-to-hydrogen as seasonal energy storage: an uncertainty analysis for optimal design of low-carbon multi-energy systems. Applied Energy **274**, 115197 (2020) https://doi.org/10.1016/j.apenergy.2020.115197

[41] Badey, Q.: Étude des mécanismes et modélisation du vieillissement des batteries lithium-ion dans le cadre d'un usage automobile. Theses, Université Paris Sud - Paris XI (March 2012). https://theses.hal.science/tel-00693344 Accessed 2023-03-16

[42] Couture, T., Gagnon, Y.: An analysis of feed-in tariff remuneration models: Implications for renewable energy investment. Energy Policy **38**(2), 955–965 (2010) https://doi.org/10.1016/j.enpol.2009.10.047

[43] Boennec, C.: Scenario data and full code associated with the article: Comparison of battery models integrating energy efficiency and aging for the design of microgrids. Zenodo (2023). https://doi.org/10.5281/zenodo.8016739

[44] Ratnam, E.L., Weller, S.R., Kellett, C.M., Murray, A.T.: Residential load and rooftop pv generation: an australian distribution network dataset. International Journal of Sustainable Energy **36**(8), 787–806 (2017) https://doi.org/10.1080/14786451.2015.1100196

Appendix A Scenario profiles

16 distinct one-year scenarios were generated using a Markov approach. The profiles are generated by applying the method from [33] on the Ausgrid distribution network data set, specifically on 20 customers for whom we have 3 years of data at 30-minute intervals. A deeper analysis of this data set is available in [44]. The demand profiles are an aggregation of 5 artificial profiles, implying that the demand corresponds to 5 households.

Each scenario is then duplicated over 20 years to enable simulations over the system's time horizon. Fig. A1 and Fig. A2 allow the visualization of the initial annual data profiles, which are replicated for each scenario. The fact of correlating the years is debatable, as it is rather unrealistic, but we made this choice to allow a better differentiation of the input scenarios from the robust optimization problem, given the small number used in the robust design process (only 16). Using profiles synthesized directly over 20 years with

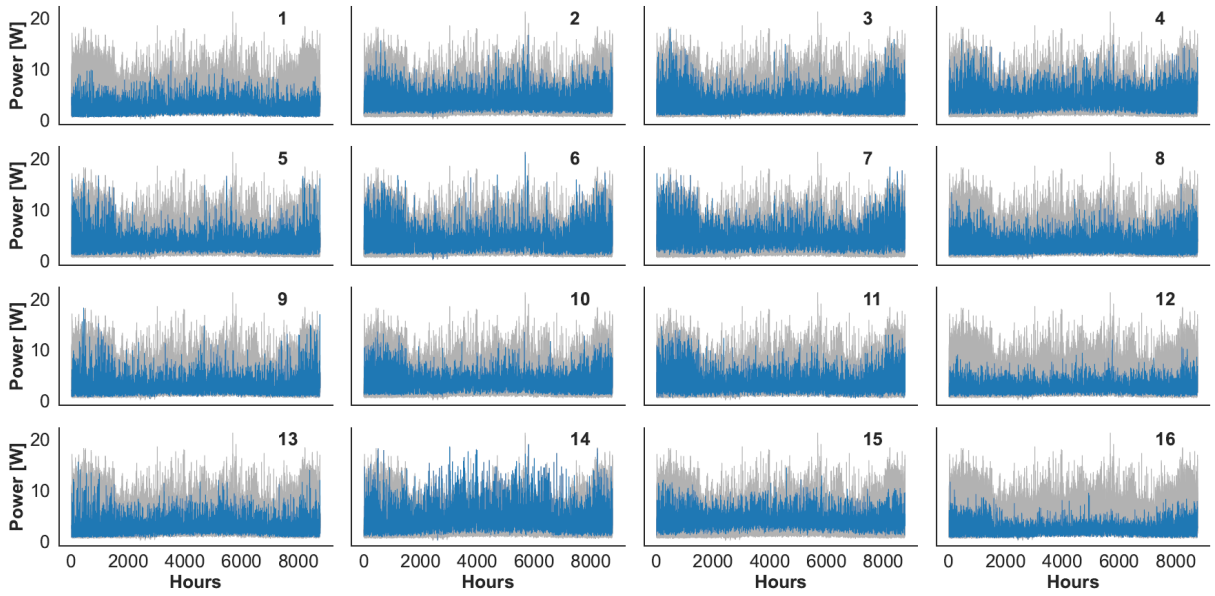

Fig. A1 Electricity load profile visualization for every yearly scenarios. The blue line represents the load profile for the corresponding panel, while the light gray lines in the background depict the profile of the other scenarios.

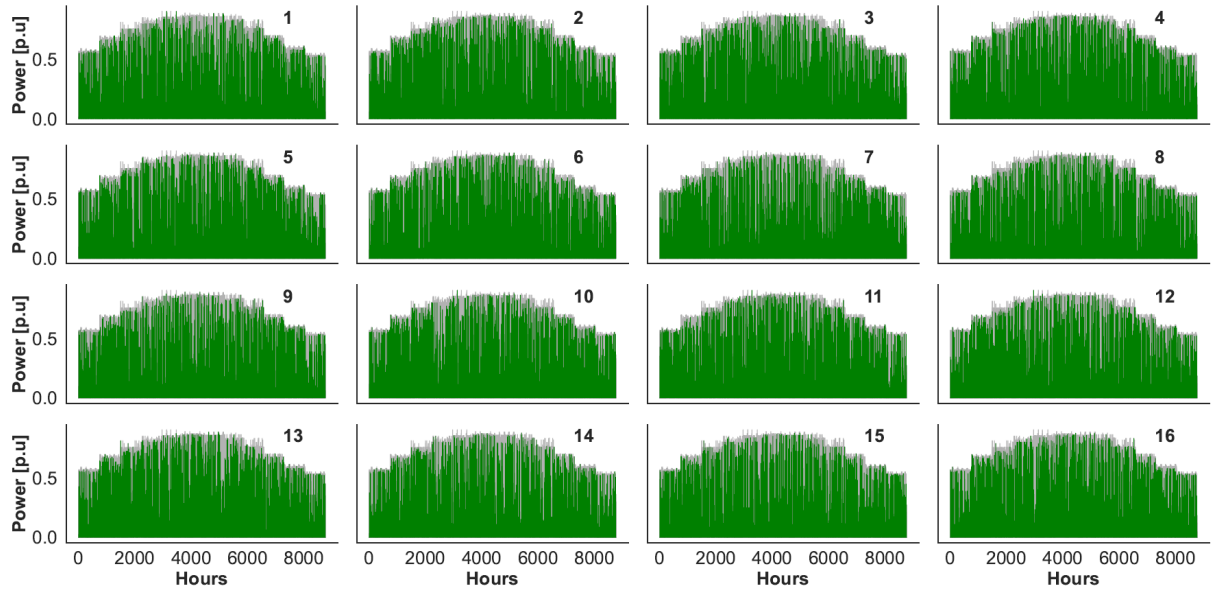

Fig. A2 Solar production profile visualization for every yearly scenarios. The green line represents the generation profile for the corresponding panel, while the light gray lines in the background depict the profile of the other scenarios.

uncorrelated years, or obtained by randomly mixing the 16 basic profiles presented here would be more realistic, but would undoubtedly be less sensitive to the variance between the different battery models we wish to characterize.